Joint Estimation of Biogeochemical Model Parameters from Multiple Experiments: A Bayesian Approach Applied to Mercury Methylation

Saubhagya S. Rathore[1*], Grace E. Schwartz[1#], Scott C. Brooks[1], Scott L. Painter[1],

[1]Environmental Sciences Division, Oak Ridge National Laboratory, Oak Ridge, Tennessee 37831-6038

[#]Current Affiliation: Department of Chemistry, Wofford College, 429 N. Church St, Spartanburg, SC 29303

[*]Corresponding Author: Email: rathoress@ornl.gov, Phone: 470-263-1189
1 Bethel Valley Road, Oak Ridge, Tennessee 37830

Keywords:

Bayesian inference, Parameter uncertainty, Mercury methylation

Highlights:

1) Jointly fitted sorption and methylation datasets allow information sharing and uncertainty propagation across process models
2) Mapping full joint distributions of parameters identified null-spaces and facilitated model simplification
3) Sediments collected from near-bank and near-center of the stream exhibited different sorption and methylation kinetics

Software and Data Availability:

The original experimental dataset is archived at Schwartz et al. (2021b). The model-data for this manuscript is archived at Rathore and Painter (2021).

Abstract:

To characterize complex biogeochemical systems, results from multiple experiments, where each targets a specific subprocess, are commonly combined. The resulting datasets are interpreted through the calibration of biogeochemical models for process inference and predictions. Commonly used calibration approaches of fitting datasets from individual experiments to subprocess models one at a time is prone to missing information shared between datasets and incomplete uncertainty propagation. We propose a Bayesian joint-fitting scheme addressing the above-mentioned concerns by jointly fitting all the available datasets, thus calibrating the entire biogeochemical model in one go using Markov Chain Monte Carlo (MCMC). The identification of null spaces in the parameter distributions from MCMC guided the simplification of certain subprocess models. For example, fast kinetic sorption was replaced by equilibrium sorption, and Monod demethylation was replaced by first-order demethylation. Joint fitting of datasets resulted in complete uncertainty propagation with parameter estimates informed by all available data.

1. Introduction:

Many stream ecosystems are under stress due to contamination driven by anthropogenic activities. In particular, trace metals such as mercury, lead and cadmium released from industrial activities pose a serious threat to human and ecosystem health because of their toxicity even at minimum levels and potential of bioaccumulation (Chen and Folt, 2000; Evers et al., 2007; Goodyear and McNeill, 1999; Horowitz, 1991; Mason et al., 2000; Ward et al., 2010). A comprehensive understanding of their transformation in the environment requires considerations of the complex interplay between physical, chemical and biological processes at different spatial and temporal scales. Carefully designed field and laboratory experiments gather critical data about these processes. However, the usefulness of these datasets depends on their reliable interpretations. Empirical relations can fit the data well but can struggle to extrapolate due to a lack of mechanistic underpinnings. Process-based biogeochemical models are developed and calibrated using the experimental data for mechanistically rich process inferences and predictions. There are generally multiple candidate biogeochemical models available to fit the data, e.g., first-order kinetics, equilibrium, Monod, and Tessier. All these models are upscaled phenomenological descriptions of complex biogeochemical processes and do not perfectly represent the biogeochemical system, since the "true" model is unknown (Neumann and Gujer, 2008). Typically, based on preliminary data analysis and expert knowledge, a model is proposed and calibrated to estimate model parameters. However, often initially proposed mechanistic models are overparameterized, needing data-driven methods for model simplification and unique parameter estimates. Commonly used approaches in biogeochemical modeling and calibration are prone to underutilization of the data available from multiple experiments, incomplete uncertainty quantification, and model overparameterization. Below we describe some of the challenges in interpreting data with commonly used biogeochemical modeling approaches and how we aim to address them.

Characterization of biogeochemical systems often requires multiple experiments targeting a subset of processes in the system (referred henceforth as subprocesses). For example, sorption experiments are performed separately from reaction-focused experiments in various biogeochemical applications (e.g., Haggerty et al., 2008; Lemke et al., 2014; Olsen et al., 2018; Schwartz et al., 2021a). Models for subprocesses, like sorption, are often calibrated first and the resulting best-fit parameters are kept fixed in the subsequent estimation of reaction parameters in a broader model framework. This sequential fitting scheme has two main shortcomings. First, it fails to make full use of all information. Information on subprocesses that are common to multiple experiments is not fully used when subprocess parameters are determined by analysis of one experiment and then held fixed in subsequent analyses. Second, sequential fitting fails to propagate uncertainty from one experiment to the next. For example, fixing sorption parameters when analyzing reaction experiments ignores the fact that the reaction experiments contain information about both sorption and reactions. Moreover, it fails to propagate uncertainty from the analyzed sorption experiment to the analysis of the reaction experiment. Figure 1 shows this sequential fitting scheme in a general biogeochemical model comprising three subprocesses that are calibrated sequentially. We propose that the datasets

from multiple experiments should be fitted simultaneously, thus calibrating all subprocess models together. By doing so, we leverage information sharing about subprocesses among datasets. Additionally, this joint-fitting scheme also allows uncertainty propagation among subprocess models. The surface (Kelleher et al., 2019; Knapp and Cirpka, 2017; Lemke et al., 2013; Liao et al., 2013) and subsurface (Luo et al., 2006; Zhao et al., 2018) hydrologists have previously recognized merit in this joint fitting approach. These studies fitted conservative and reactive tracer data from tracer experiments jointly rather than sequentially to leverage shared information and propagate uncertainty fully. Biogeochemical systems, typically more complex with a larger number of highly intertwined subprocesses, can particularly benefit from sharing information because of the different scales and interactions of these subprocesses captured in different experiments.

A more general problem and very relevant to biogeochemical modeling is the lack of parameter identifiability (Beck, 1987), which essentially means that significantly different parameter values can reproduce the experimental data equally well. This can result from insufficient information in the experimental data to match the model complexity or "incorrect" model structure (Marschmann et al., 2019). Although non-linear least-square schemes can yield parameters that produce a good match between simulations and experimental data in such cases, the model structure deficiency can go undetected leading to non-meaningful local uncertainty estimates and faulty process inferences (Marschmann et al., 2019; Neumann and Gujer, 2008; van Turnhout et al., 2016). Neumann and Gujer (2008) showed that bias related to model-structure in environmental models can be diagnosed through analysis of residuals from non-linear regression schemes. Marschmann et al. (2019) used information geometry to identify model structure limitations and reduce the model complexity in mechanistically rich biogeochemical models suffering from the lack of parameter identifiability. With the advancements in computational capabilities, computationally intensive Bayesian inverse modeling have become accessible to widespread applications including biogeochemical modeling. Mapping full joint distributions of parameters in Bayesian approach can reveal parameter uncertainties, sensitivities, interactions and potential null spaces, which can guide model improvements. Arhonditsis et al. (2008) applied Bayesian calibration using Markov Chain Monte Carlo (MCMC) to rigorously quantify parameter and predictive uncertainty in aquatic-biogeochemical models. Zhang and Arhonditsis (2009), using synthetic aquatic-biogeochemistry datasets, demonstrated the strength of the Bayesian approach in transferring information across systems as priors in a hierarchical calibration scheme. van Oijen et al. (2011) calibrated four different biogeochemical models for Norway spruce forest using MCMC. They compared models through "integrated likelihood" values of the estimated parameter distributions. van Turnhout et al. (2016) developed a toolbox with Bayesian-inference-based criteria for selecting optimal reaction network in Municipal Solid Waste landfills. Davoudabadi et al. (2021) used particle-filter-based advanced Bayesian methods to calibrate high complexity state-space models with soil-carbon sequestration as an example.

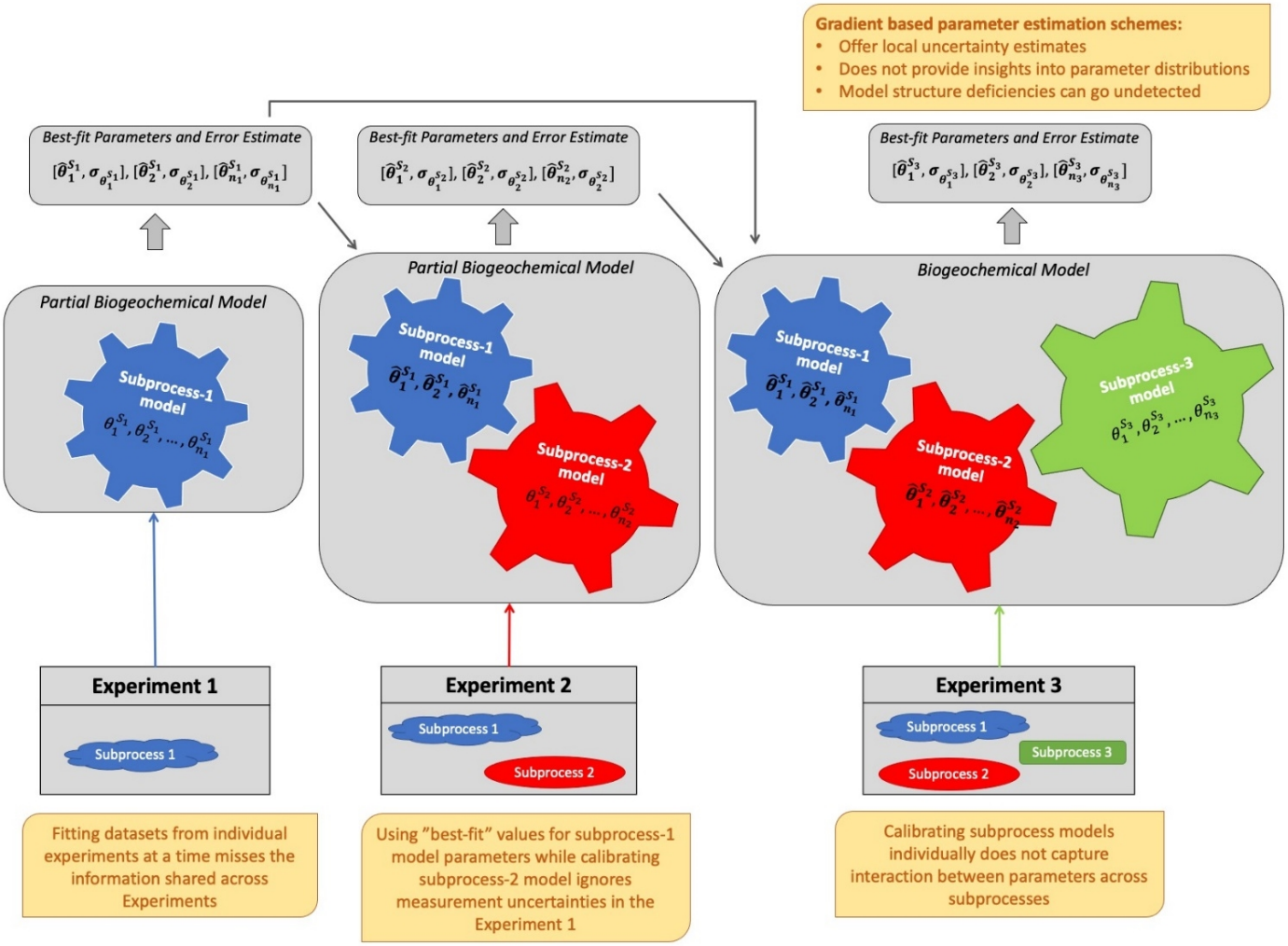

Figure 1: Sequential calibration of individual subprocesses and gradient-based parameter estimation schemes commonly used to calibrate complex biogeochemical models have several shortcomings, which were encountered by Schwartz et al. (2021a). $\theta_j^{S_i}$ represents j^{th} parameter (out of total n_i parameters) of subprocess model S_i

In this paper, we present a holistic framework of Bayesian joint fitting for biogeochemical models leveraging information from multiple experiments, treating uncertainty rigorously, and detecting potential parameterization deficiencies. This approach broadly has two facets. First, we propose that the datasets from multiple experiments should be fitted simultaneously, thus calibrating all subprocess models together. By doing so, we are informing each subprocess model using all the available datasets involving that particular subprocess. Additionally, this joint-fitting scheme also allows uncertainty propagation among subprocess models and different datasets. Second, we map the full joint distribution of parameters using the advanced Markov Chain Monte Carlo (MCMC) method. This approach not only yields robust global uncertainty estimates and but can also identify model deficiencies causing the lack of parameter identifiability. We apply the proposed workflow to a recently published mercury

methylation dataset (Schwartz et al., 2021b) to improve data interpretation and advance process inferences.

Characterization of mercury methylation processes, a use case in this paper, is of significantly high importance as methylmercury (MeHg) poses a great threat to humans and wildlife (Eckley et al., 2020). Occurring in the environment as a natural and anthropogenic pollutant, Hg is methylated to form the neurotoxin MeHg through microbially mediated processes (Clarkson et al., 2003). MeHg ingestion even at a low level has adverse impacts on the development of children. MeHg can get biomagnified in aquatic food webs which makes it particularly concerning (Mergler et al., 2007). Significant experimental and modeling efforts have been made to understand mercury methylation dynamics (Avramescu et al., 2011; Hintelmann et al., 2000; Jonsson et al., 2012; Liem-Nguyen et al., 2016; Mitchell and Gilmour, 2008; Olsen et al., 2018; Rodŕıguez Martín-Doimeadios et al., 2004; Schwartz et al., 2019).

Traditionally, first-order reversible kinetics have been used to model mercury-methylation (Hintelmann et al., 2000), however, apparent non-first order kinetic behavior has often been observed in mercury methylation-demethylation data (Avramescu et al., 2011; Jonsson et al., 2012; Olsen et al., 2018). Olsen et al. (2018), studying mercury methylation in periphyton biofilms, suggested that the apparent non-first order behavior does not necessarily imply non-first order kinetics, but can result from other competing processes making Hg and MeHg unavailable for methylation and demethylation, respectively. They proposed the Transient Availability Model (TAM) accounting for competing processes like multisite kinetic sorption of Hg and MeHg and reduction of Hg. Schwartz et al. (2022) extended the TAM framework to aquatic sediment systems to model mercury methylation on two disparate sediments from East Fork Poplar Creek (EFPC) in Oak Ridge, TN, USA. TAM application by Schwartz et al. (2022) considered fully kinetic competing processes for bioavailability with first-order methylation-demethylation for one sediment type, and reversible Monod kinetics for another. With the sequential fitting of sorption and methylation datasets and a gradient-based scheme for parameter estimation, they reproduced experimental data well but obtained non-meaningful error estimates for certain parameters. Using the novel mercury-methylation dataset (Schwartz et al., 2021b), we implement the proposed parameter estimation workflow in the TAM framework.

Olsen et al. (2018) and Schwartz et al. (2022) studied biologically mediated methylation of mercury (Hg) to the neurotoxin methylmercury (MeHg) on periphyton film and colonized sediments, respectively. Both studies fitted sorption experiment datasets first to estimate sorption parameters, which were then fixed while estimating methylation-demethylation parameters fitting datasets from methylation experiments. However, it is important to recognize that these processes are not independent and methylation-demethylation datasets also contain information about the sorption processes, which is not leveraged in this sequential fitting approach. Additionally, because of using the “best fit” values of sorption parameters, the estimates of methylation-demethylation parameters ignore uncertainties in sorption datasets. In our approach, sorption and methylation datasets are fitted simultaneously and respective parameters are jointly estimated, thus addressing the above-described concerns.

For the uncertainty-aware parameter estimation, Olsen et al. (2018) and Schwartz et al. (2022) adopted a gradient-based local optimization scheme, which works well in unimodal smooth parameter spaces but can suffer in multimodal or other atypical parameter spaces. Additionally, under such schemes, other model-structure-related issues like overparameterization may go undetected. We adopt a Bayesian approach using MCMC, a global-search scheme yielding a full joint distribution of parameters. The obtained parameter distributions are expected to guide model improvements in addition to offering robust uncertainty estimates.

With the proposed parameter estimation workflow of Bayesian joint fitting, we aim to improve the interpretation of the rich mercury methylation dataset by Schwartz et al. (2021b). The proposed workflow is easily transferable to other complex biogeochemical systems characterized through multiple experiments for reliable parameter estimates, process inferences, and predictions.

2. Overview of Experiments and Datasets

Here we provide a brief overview of the study site and experiments. For more information about the site see Brooks and Southworth (2011); Riscassi et al. (2016) and for experimental details, see Schwartz et al. (2022). Schwartz et al. (2022) collected sediments from EFPC, that have legacy mercury contamination, and performed sorption and mercury methylation experiments to characterize and quantify their methylation and demethylation potential and associated physical, chemical, and microbial processes. Two contrasting sediment types were collected for use in laboratory studies. Sediment 1 – rich in organic matter, relatively anoxic fine sand predominant along the stream edge, and Sediment 2 – a medium to coarse sand lower in organic carbon and less metabolically active than Sediment 1, and predominant in the center of the channel.

For Hg and MeHg sorption experiments, isotopically labeled ^{201}Hg or $Me^{202}Hg$ were added to sediment-creek water suspension under air and placed on a reciprocating shaker. The number of time points at which samples were collected for Hg are 12 and 14 for Sediment 1 and for Sediment 2, respectively, and for MeHg, 14 and 15, respectively. Triplicate samples were sacrificed at each time point. In the Hg sorption experiment, Hg in the aqueous phase, total solid-phase Hg, and Hg(0) were quantified at different time points. Under the oxic conditions of the Hg sorption experiments Hg methylation, an obligately anaerobic microbial process, did not occur. In the MeHg sorption experiments, aqueous $Me^{202}Hg$ quantified at different time points from triplicate samples and total $Me^{202}Hg$ in the system was quantified at select time points to verify the lack of demethylation of the added isotope (Schwartz et al., 2022).

Mercury-methylation experiments were conducted on carefully prepared anoxic sediment slurry microcosms. Three treatments were established, one spiked with ^{201}Hg to monitor methylation via production of $Me^{201}Hg$, the second spiked with $Me^{202}Hg$ to monitor demethylation via loss of $Me^{202}Hg$, and treatment with no spike added to monitor other biogeochemical parameters of interest (e.g., Fe(II), sulfide) because the Hg and MeHg analyses were full consumptive and destructive. The experiment for Sediment 2 was run longer because

of the low activity initially measured in those sediments. The number of timepoints at which samples were collected is 4 and 3 for Sediment 1 and Sediment 2, respectively. Three microcosms from each treatment were destroyed at each time point for Hg and MeHg analysis. The resulting datasets from mercury-methylation experiments are total $Me^{201}Hg$ and $Me^{202}Hg$ at each time point (Schwartz et al., 2022).

3. Bayesian Joint-Fitting Approach

The data from the experiments by Schwartz et al. (2022) captures information about the biogeochemical processes controlling methylation of mercury on colonized river sediments. Models under the TAM framework are proposed for these biogeochemical processes and calibrated to match the experimental data allowing us to make process inferences and develop prediction capabilities. Experience from the interpretation of mercury methylation datasets by Schwartz et al. (2022) reveals several shortcomings of commonly used biogeochemical model calibration practices which we discussed in the Introduction section (Figure 1).

Our approach leverages information shared among experiments by joint calibration of subprocesses using all the available datasets. Additionally, full joint distribution of parameters is mapped to get robust uncertainty estimates and detect potential model-structure deficiencies. In Figure 2, we present a schematic of our Bayesian joint-fitting scheme and the advantages of different facets of the scheme. In the following sub-sections, we describe different models considered for sorption and methylation, provide Bayesian formulation, and details of MCMC application.

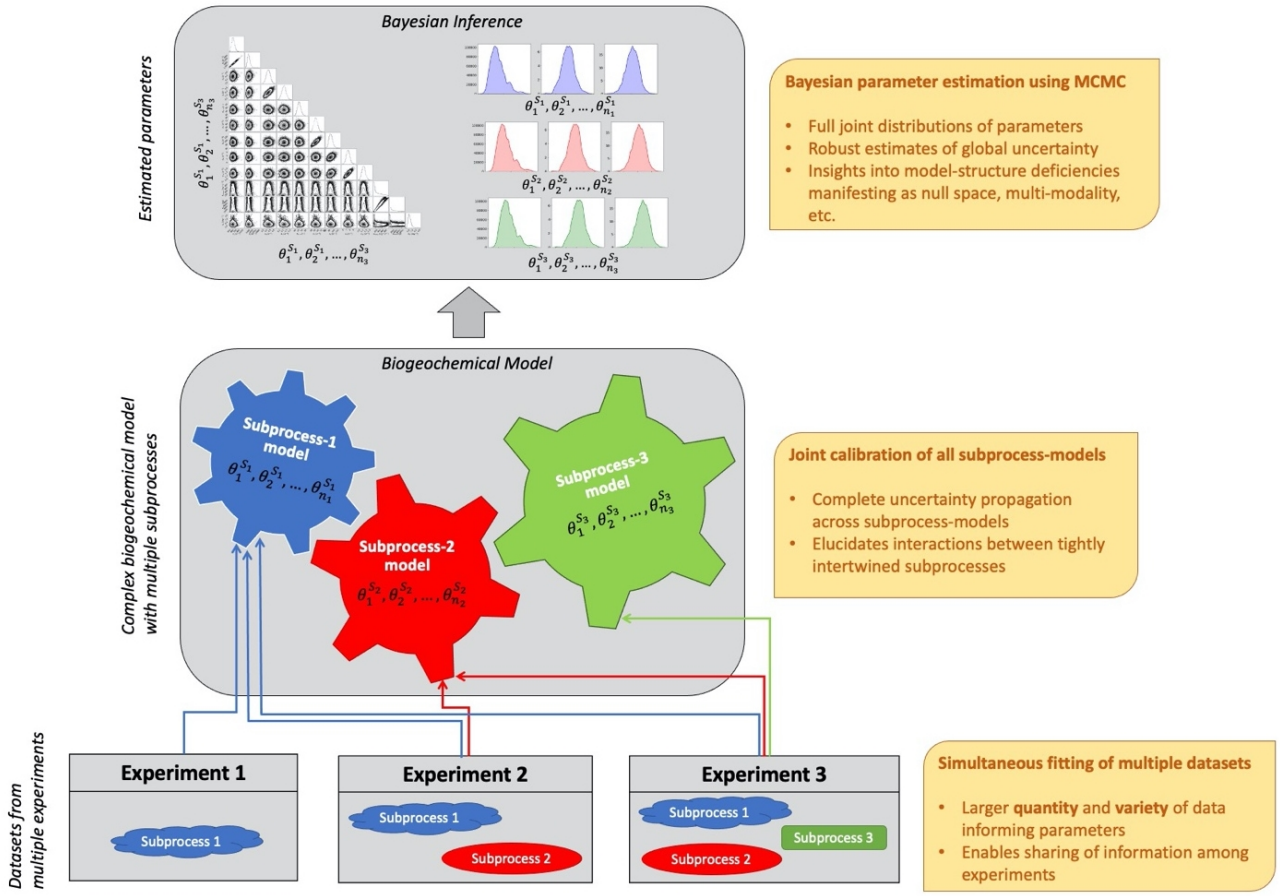

Figure 2: Schematics of Bayesian joint-fitting scheme for calibrating complex biogeochemical models offer multiple advantages with efficient utilization of datasets, full uncertainty propagation and robust estimation, and detecting parameterization deficiencies

3.1. Transient Availability Model Framework

The TAM model framework developed by Olsen et al (2018) is used to describe mercury methylation. Under the TAM model framework, methylation and demethylation of mercury are strongly influenced by the availability of Hg and MeHg in the aqueous phase. Experiments suggest that the transient availability of Hg in the aqueous phase is caused by competition with two-site sorption and reversible reduction of aqueous mercury into elemental mercury, while that of MeHg is governed by competition with two-site sorption. Figure 3 shows schematics of the general TAM model framework.

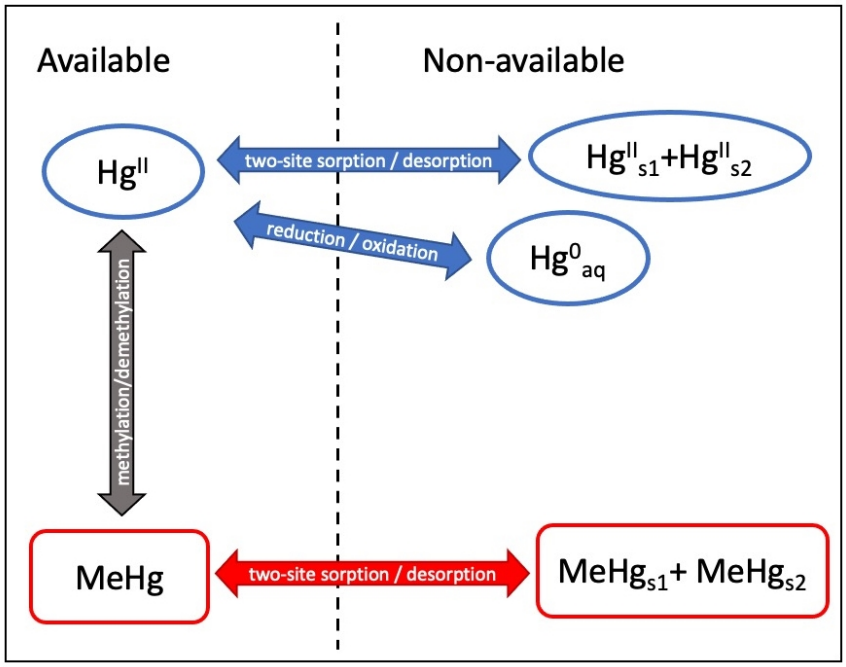

Figure 3: Schematics of TAM framework for mercury methylation representing competing biogeochemical processes (modified from Olsen et al. (2018))

For both types of sediments, Schwartz et al. (2022) modeled two-site sorption as fast and slow first-order reversible kinetic sorption. Similarly, the reduction of Hg(II) to Hg(0) was also modeled as a first-order reversible kinetic process. For Sediment 1, both methylation and demethylation were modeled using Monod kinetics. For Sediment 2, methylation and demethylation were modeled using first-order kinetics. The uncertainty-aware parameter estimation was performed using a gradient-based scheme (*nlinfit* in Matlab) yielding locally optimal parameter values with first-order error estimates. Schwartz et al. (2022) found large parameter uncertainties and non-unique solution (sensitive to initial values) for Monod kinetics in Sediment 1. Additionally, when they applied Monod kinetics in Sediment 2, the parameter estimation scheme failed to converge without giving any clear insights into the defects in the considered parameterization. This is not surprising as potential overparameterization-related model-structure deficiencies can go undetected with gradient-based non-linear fitting schemes.

In this study, we first implement the proposed Bayesian joint-fitting scheme, i.e. jointly calibrating sorption and methylation models using MCMC with TAM model in Schwartz et al. (2022). Thereafter, based on the insights from the resulting joint posterior distributions, we aim to improve the TAM model framework for both Sediment 1 and Sediment 2 to explain the experimental data better and obtain robust uncertainty estimates. The system of ODEs in TAM reaction network are solved using *odeint* from *scipy.integrate* package in Python which uses lsoda from FORTRAN *odepack* library.

3.2. Bayesian Formulation

We estimate all parameters in the TAM framework simultaneously by fitting datasets from sorption and methylation experiments together. We adopt the Bayesian approach to estimate distributions of TAM parameters conditioned on the measurements. Measurements from Hg sorption, MeHg sorption, and methylation experiments are represented by vectors $\boldsymbol{C}_1^{meas}$, $\boldsymbol{C}_2^{meas}$, and $\boldsymbol{C}_3^{meas}$, respectively. Measurements for model calibration are triplicate averages at each time point. Collectively, all model parameters can be represented by vector $\boldsymbol{\theta}$ and measurements by $\boldsymbol{C}^{meas}$. Using Bayes' theorem, conditional probability density function $p(\boldsymbol{\theta}|\boldsymbol{C}^{meas})$ can be given as:

$$p\left(\boldsymbol{\theta} \mid \boldsymbol{C}^{meas}\right) \propto p(\boldsymbol{C}^{meas}|\boldsymbol{\theta})p(\boldsymbol{\theta}) \tag{1}$$

where $p(\boldsymbol{C}^{meas}|\boldsymbol{\theta})$ is the likelihood of the measurements $\boldsymbol{C}^{meas}$ given the parameter set $\boldsymbol{\theta}$, which represents the constraints imposed by $\boldsymbol{C}^{meas}$ on $\boldsymbol{\theta}$. The $p(\boldsymbol{\theta})$ is the probability density function representing the prior knowledge about parameters. Probability $p(\boldsymbol{C}^{meas}|\boldsymbol{\theta})$ is composed of contributions from individual experiments as:

$$p\left(\boldsymbol{C}^{\boldsymbol{meas}} \mid \boldsymbol{\theta}\right) = \prod_{i=1}^{3} p\left(\boldsymbol{C}_i^{\boldsymbol{meas}} \mid \boldsymbol{\theta}\right) \tag{2}$$

$\boldsymbol{C}_i^{meas}$ for all experiment is assumed to follow multi-gaussian distribution:

$$p\left(\boldsymbol{C}_i^{meas} \mid \boldsymbol{\theta}\right) = \frac{1}{\sqrt{(2\pi)^n |\boldsymbol{\Sigma}_\mathrm{i}|}} \exp\left(-\frac{1}{2}\left(\boldsymbol{C}_i^{meas} - \boldsymbol{C}_i^{sim}\right)^T \boldsymbol{\Sigma}_\mathrm{i}^{-1} \left(\boldsymbol{C}_i^{meas} - \boldsymbol{C}_i^{sim}\right)\right) \tag{3}$$

where, $\boldsymbol{\Sigma}_\mathrm{i}$ represents the covariance matrix of the measurements, $|\boldsymbol{\Sigma}_\mathrm{i}|$ represents its determinant, and n is the number of time points in the dataset. We assume uncorrelated measurement errors resulting in a diagonal $\boldsymbol{\Sigma}_\mathrm{i}$ matrix with measurement variances as diagonal elements. We assume uniform priors for all parameters with a reasonable range based on domain knowledge. We do not have any additional information to assume non-uniform priors. For cases when parameter distribution hit the boundary of the parameter space, analysis is repeated with expanded range a few times to ensure there is no additional mode beyond range. We assume a homoscedastic error model and evaluate pooled variance for each dataset (i.e., variance of different populations with different means with presumably same variance). This is a reasonable choice as triplicate variances did not show consistent trend with time. It is important to note, however, that pooled variance calculated this way is still uncertain because of small sample size. We ignore the uncertainty in variance here but note it could be estimated in a more robust way by taking the variance as a hyperparameter that is sampled along with main model parameters.

For each case, we plotted the distribution of residuals of model fit and found them to be unimodal, almost symmetric and gaussian, except at early timestep in one of the cases. Hence, our assumption of gaussian likelihood is reasonable for these datasets. The example plots of residual distributions for methylation and demethylation in both types of sediments are provided in the Appendix-B.

3.3. MCMC Implementation

For most practical cases, it is almost impossible to analytically derive the joint distributions of parameters. Hence, we use the MCMC technique, a family of algorithms designed to approximate posterior distributions of variables of interest by drawing samples from their derived distributions. MCMC has benefitted many fields where posterior inferences about complex systems in the Bayesian framework are desired (Vrugt et al., 2008). MCMC offers globally optimal solutions with full joint distributions of parameters. This allows for the quantification of parameter uncertainties rigorously, assessment of model structure adequacy, and potential for model improvements.

In this study, we use PyDREAM (Shockley et al., 2018), a python implementation of the DREAM(ZS) (Laloy and Vrugt, 2012) algorithm, which is one of the most advanced adaptions of DiffRential Evolution Adaptive Metropolis (DREAM) (Vrugt et al., 2008). DREAM is a multi-chain MCMC with the automatic adaption of step size and direction of sampler movement. DREAM(ZS) stores past states in archives which are then used to propose new positions making it highly efficient with quick convergence and fewer number of chains needed. With a range of proposal maneuvers, DREAM(ZS) can sample from challenging parameter spaces like multimodality and highly correlated parameters. Key inputs to DREAM(ZS) algorithm includes number of differential pairs equals to 3, gamma levels to 4, probability of unity gamma to 0.2 and probability of snooker step to 0.1. For more details about these options, refer to Shockley et al. (2018) and Laloy and Vrugt (2012).

We provide in the supporting information a modular python workflow in which each experiment is modeled in a separate python script and is accessed by the main python script performing MCMC. Therefore, datasets from additional experiments can be conveniently included in the MCMC analyses. The MCMC results are post-processed, analyzed, and visualized in Jupyter notebooks enabling an efficient and self-documenting workflow. The model-data files are archived at Rathore and Painter (2021).

4. Results and Discussion

MCMC runs were performed using 10 parallel communicating chains with at least 25,000 generations per chain after chains had converged. The convergence of chain is tested using Reduction Factor ($\hat{R}$) criteria by Gelman and Rubin (1992) which when below 1.2 indicates the chain convergence. Plots for the evolution of $\hat{R}$ with the progression of chains for each MCMC run can be found in the SI. The posterior distributions of estimated parameters were summarized using at least 250,000 parameter sets yielding a robust estimation. First, we present parameter estimation with models of Schwartz et al. (2022). Based on the insights into

the parameter space, we improve the model structure and discuss process inferences. Equations for final improved models are provided in the Appendix-A.

4.1. Bayesian Joint-Fitting for Transient Availability Model by Schwartz et al. (2022)

4.1.1. Model Description

Figure 4(a) depicts models considered by for fitting sorption and methylation experiment data sequentially for both Sediments 1 and 2. Hg sorption experiment is modeled using three first-order reversible kinetic processes, namely, sorption-desorption on fast sites (Hg^{II}_{fast}) with parameters k_1 $[T^{-1}]$ and k_2 $[T^{-1}]$, sorption-desorption on slow sites (Hg^{II}_{slow}) with parameters k_3 $[T^{-1}]$ and k_4 $[T^{-1}]$, and first-order reversible kinetic reduction to Hg^{0}_{aq} with parameters k_5 $[T^{-1}]$ and k_6 $[T^{-1}]$. MeHg sorption is modeled using first-order reversible kinetic fast-site sorption with parameters k_7 $[T^{-1}]$ and k_{10} $[T^{-1}]$ and slow-site sorption with parameters k_9 [T^{-1}] and k_{10} $[T^{-1}]$. They fitted Hg and MeHg models to respective experimental data and reported best-fit parameters and quantified uncertainty as 5th and 95th confidence intervals. Thereafter, the mercury methylation model under the TAM framework was calibrated to estimate methylation and demethylation parameters keeping sorption parameters fixed as best-fit values estimated previously. In Sediment 1, Monod kinetics was used to model methylation and demethylation. For methylation, k_{mmax} $[MT^{-1}]$ and K_{mhs} $[M]$ denote maximum reaction rate and half-saturation constant, respectively. Similarly, for demethylation, Monod parameters are denoted as $k_{dmax}[MT^{-1}]$ and K_{dhs} $[M]$. Monod reactions exhibit first-order behavior at concentrations significantly smaller than K_{hs} and zeroth-order behavior at concentrations significantly greater than K_{hs}. In Sediment 2, reversible first-order kinetics was used for methylation and demethylation with rate constants k_m $[T^{-1}]$ and k_d $[T^{-1}]$, respectively.

We estimate all parameters together by fitting seven datasets from three experiments (described in section 2) simultaneously using MCMC to obtain full posterior joint distributions. Figures 4(b) and 5(b) maps experimental datasets to the parameters they are informing. This allows for a rigorous treatment of uncertainty in all parameters and full utilization of the information shared among available datasets. In section 4.1.2, joint distributions of parameters of the model by Schwartz et al. (2022) obtained from MCMC are presented for both sediment types. Marginal distributions and predictive uncertainty plots are provided in the SI.

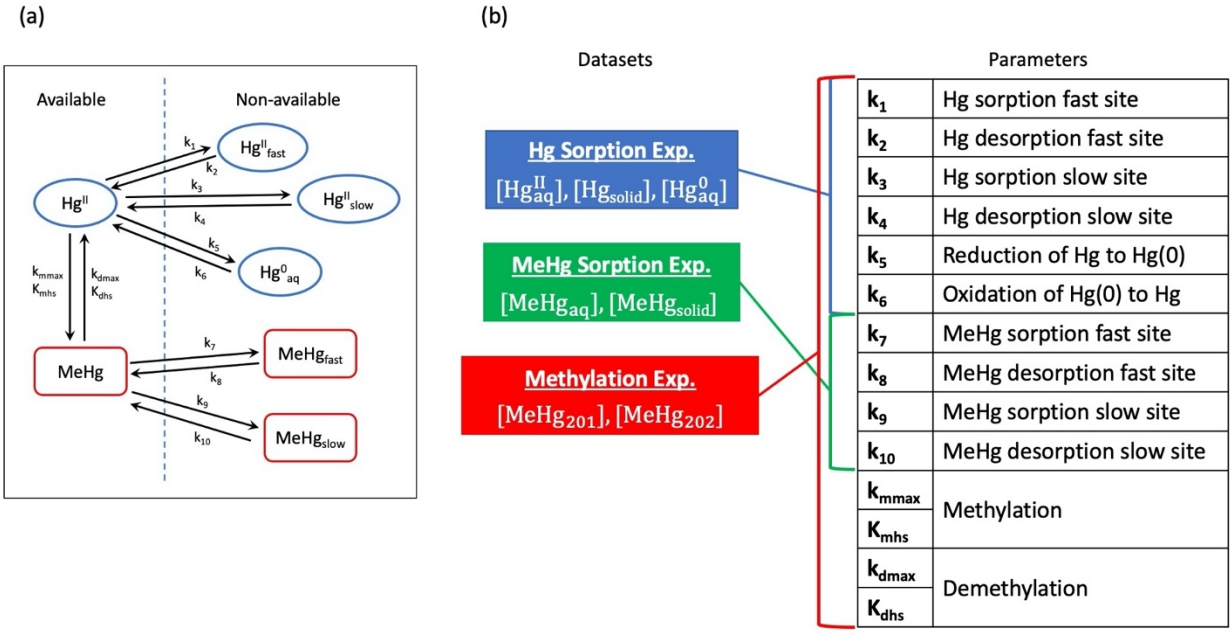

Figure 4: Reversible first-order kinetics for Hg and MeHg two-site sorption, Hg reduction, and reversible Monod kinetics for methylation considered by Schwartz et al. (2022) for Sediment 1

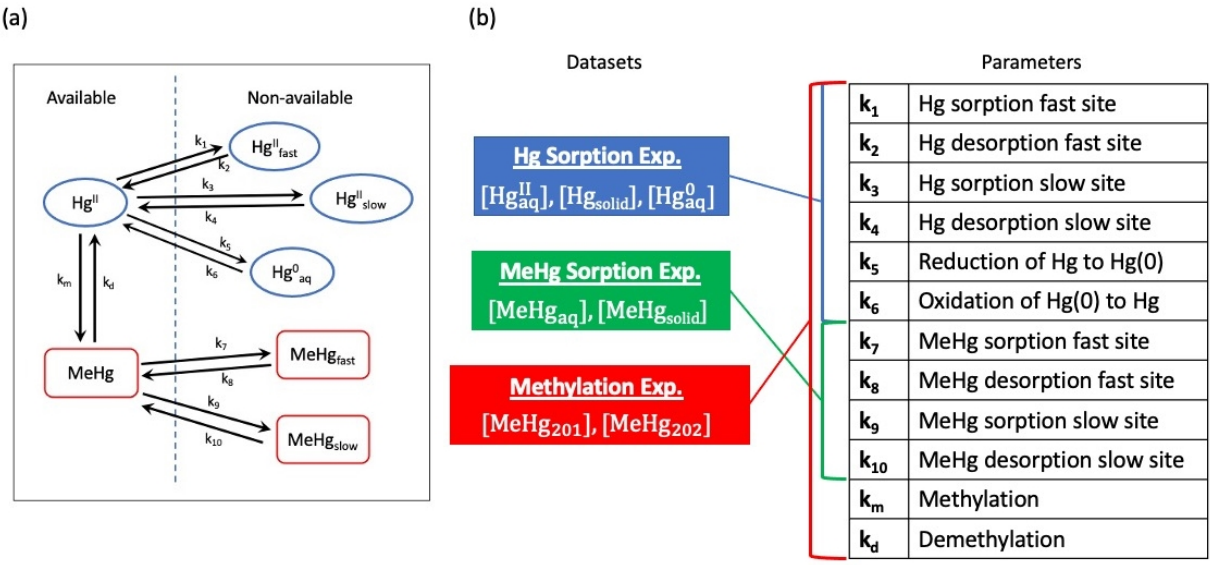

Figure 5: Reversible first-order kinetics for Hg and MeHg two-site sorption, Hg reduction, and methylation considered by Schwartz et al. (2022) for Sediment 2

4.1.2. Joint Distribution of Parameters

Figure 6 and Figure 7 present MCMC results for Sediment 1 and Sediment 2, respectively, as individual parameter histograms and pairwise joint distributions. $\hat{R}$ for the converged chains for all the parameters was approximately equal to 1 in both cases of sediment types. For Sediment

1 the distributions of parameters are unimodal with reasonable uncertainty, except for Hg reduction and the Monod parameters. The marginal distributions of the Hg reduction parameters are almost non-informative. Their joint distribution appears to be unconstrained with a strong linear correlation suggesting that the parameter space contains a null space defined by a distinctive k_6/k_5 ratio (distribution presented in Figure 6). This strongly suggests that for the considered system, Hg reduction should be modeled as an equilibrium reaction. Similarly, Monod parameters for demethylation, k_{dmax} and K_{dhs}, also span a null space defined by their distinct ratio, suggesting that the experimental data can be explained by a simpler first-order kinetic model for demethylation. Monod methylation parameters, k_{mmax} and K_{mhs}, also exhibit strong linear correlation and high uncertainty with a thick tail, but with some central tendency as unique peaks. Because of this null space in demethylation-parameter distributions and highly skewed non-gaussian methylation-parameter distributions, Schwartz et al. (2022) obtained very large uncertainty estimates and non-unique solutions for Monod methylation-demethylation parameters.

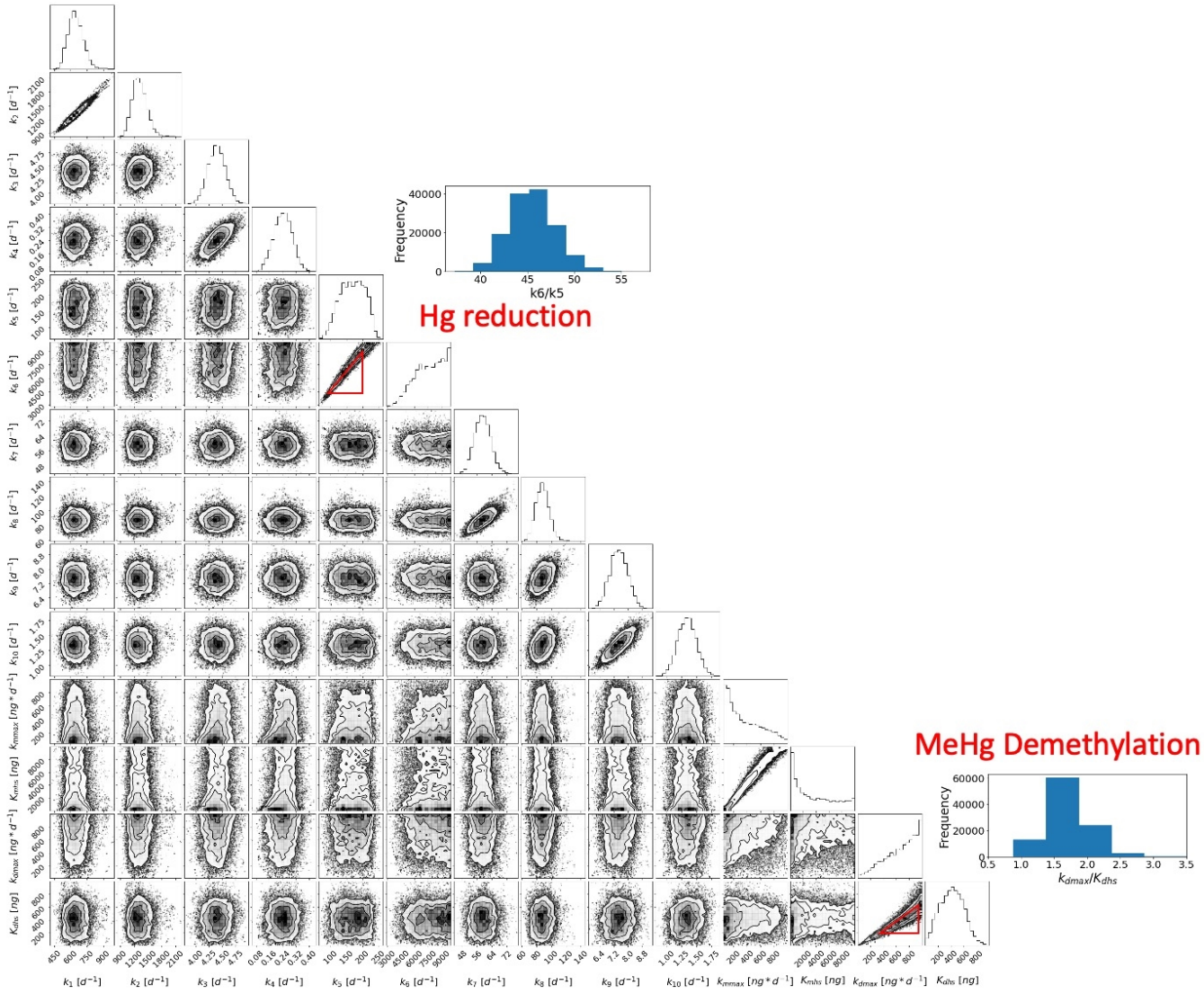

Figure 6: Joint distributions of parameters obtained from MCMC for model framework proposed by Schwartz et al. (2022) for Sediment 1

For Sediment 2, the parameters for fast sorption for Hg (k_1 and k_2), Hg reduction (k_5 and k_6) and fast sorption of MeHg (k_7 and k_8) were non-informative and unconstrained, spanning a null space characterized by a distinct ratio of forward to reverse rate constants (distributions of ratios shown in Figure 7). This favors replacing the reversible kinetic models for Hg reduction and fast sorption of Hg and MeHg with corresponding equilibrium models. The non-linear least-square fitting scheme as adopted in Schwartz et al. (2022) does not offer such insights into parameter space. The "best-fit" parameters for these subprocess models by Schwartz et al. (2021a) are one of the many equally good possibilities in the null space, and their local error estimates stem from perturbations around the "best-fit" parameters. In section 4.2, based on the insights obtained from MCMC results, improved models are proposed, and parameter estimation is performed for new models.

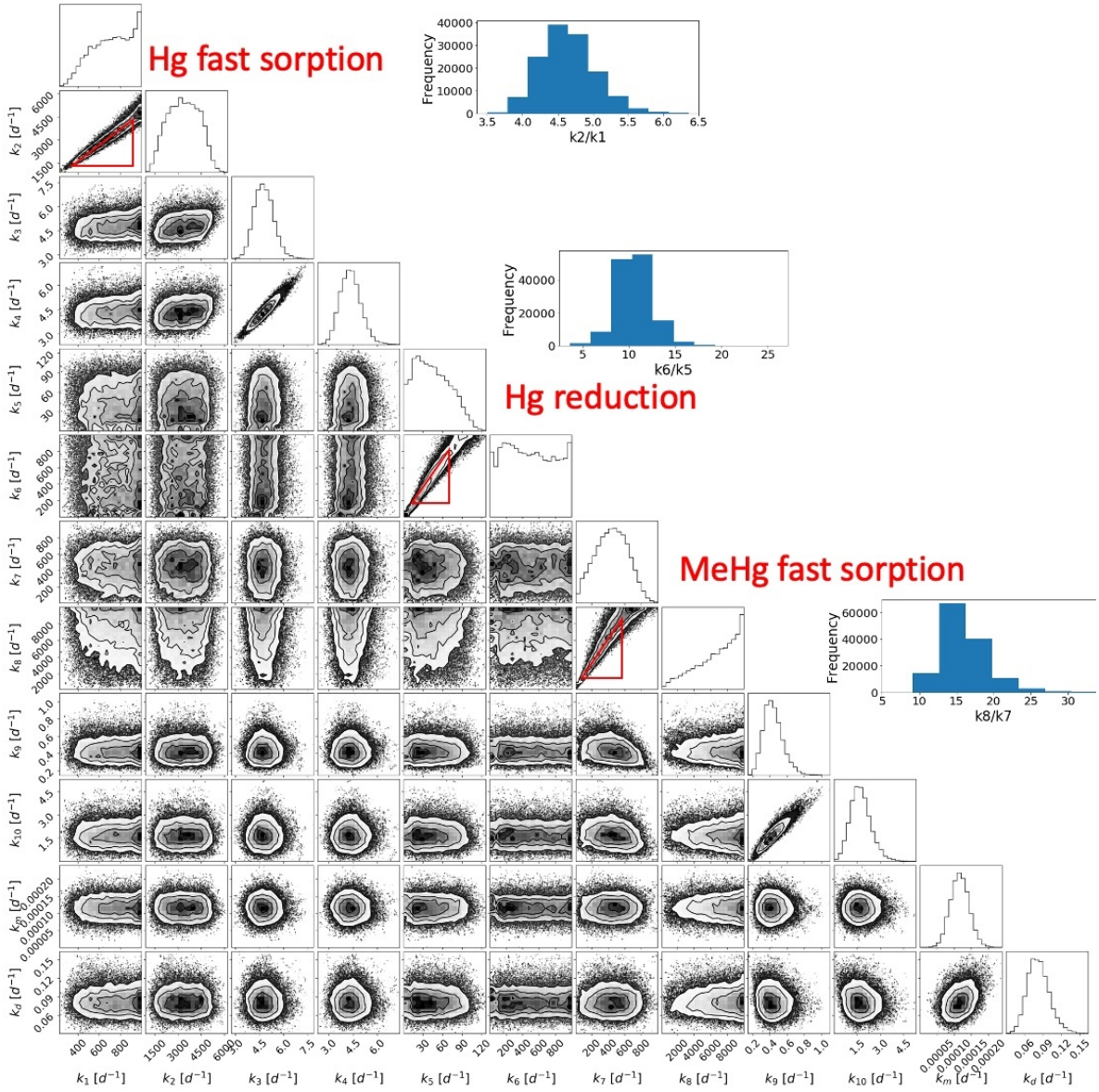

Figure 7: Joint distributions of parameters obtained from MCMC for model framework proposed by Schwartz et al. (2022) for Sediment 2

4.2. Bayesian Joint Fitting for Updated Models

Based on the insights gained from the MCMC analysis of the Schwartz et al. (2022) model, we propose improved models and perform Bayesian parameter estimation to obtain joint parameter distributions and quantify uncertainties for both Sediment 1 and Sediment 2. $\hat{R}$ for all the parameters was approximately equal to 1 in both cases of sediment types, except for k_d in Sediment 1 for which final $\hat{R}$ is equal to 1.07. Model descriptions, estimated parameters distributions, summary statistics and predictive uncertainties are presented in the following subsections.

4.2.1. Sediment 1

Under the improved model structure for Sediment 1, mercury reduction is modeled as an equilibrium process parameterized by a single parameter – the dimensionless equilibrium constant K_{5-6} [—]. Note that the subscripts of the equilibrium constant are related to the corresponding kinetic models in Figure 4 for the sake of clarity and convenience. Additionally, demethylation is modeled using first-order kinetics with a rate constant k_d $[T^{-1}]$. The model structure and estimated joint parameter distributions are presented in Figure 8. Marginal distributions are provided in SI. All parameters are estimated as unimodal distributions. Monod parameters for methylation exhibit high uncertainty with a thick tail. This ambiguity is potentially due to time-varying microbial activity due to evolving redox conditions in the sediments (Schwartz et al., 2022). The summary statistics of parameters are presented in Table 1 in the form of 5th, 25th, median, 75th, and 95th percentiles.

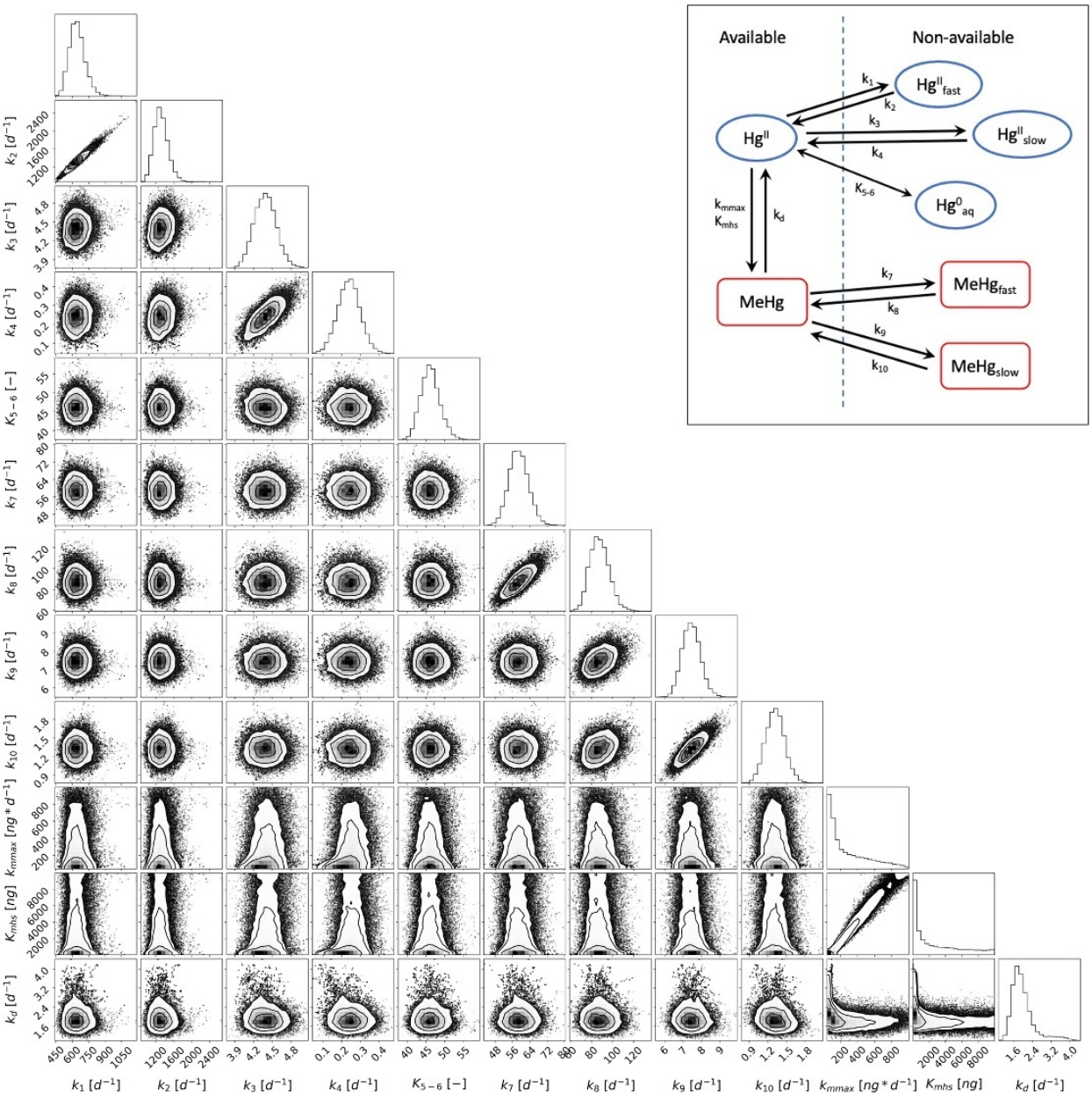

Figure 8: Model description (top right) and joint distributions of parameters obtained from MCMC for the improved model for sediment 1

Table 1: Summary statistics of parameters estimated from MCMC for the improved model for sediment 1

Parameter	5th	25th	Median	75th	95th
$k_1[d^{-1}]$	5.39e2	5.96e2	6.40e2	6.88e2	7.72e2
$k_2[d^{-1}]$	1.08e3	1.2e3	1.30e3	1.41e3	1.60e3
$k_3[d^{-1}]$	4.11	4.27	4.39	4.50	4.68
$k_4[d^{-1}]$	1.41e-1	2.00e-1	2.39e-1	2.79e-1	3.40e-1
$K_{5-6}[-]$	42.29	44.48	46.13	47.80	50.63
$k_7[d^{-1}]$	51.78	55.82	58.71	61.81	66.42
$k_8[d^{-1}]$	73.86	81.11	87.12	93.60	1.03
$k_9[d^{-1}]$	6.67	7.10	7.44	7.77	8.27
$k_{10}[d^{-1}]$	1.07	1.22	1.32	1.42	1.58
$k_{mmax}[ngd^{-1}]$	67.6	93.6	191.8	441.4	795
$K_{mhs}[ng]$	35.6	282.3	1426.2	4671.5	8874.7
$k_d[d^{-1}]$	1.43	1.68	1.88	2.16	3.08

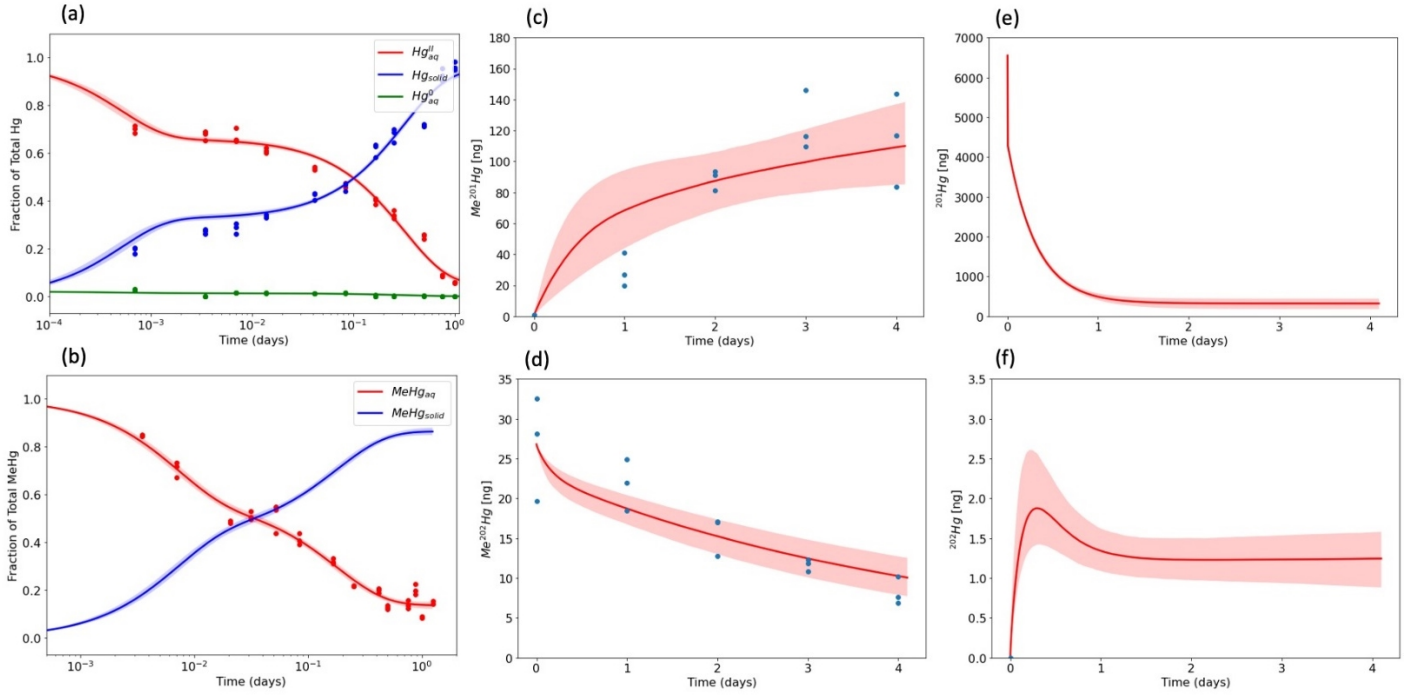

Figure 9: Median (solid line), bands of 2.5th and 97.5th percentiles (shaded region) of predictions and experimental data (solid dots) for Hg sorption and reduction (gaseous phase is not shown) (a), MeHg sorption (b), and methylation-demethylation experiment (c - d), along with the predicted concentration history of total dissolved of ^{201}Hg (e) and ^{202}Hg (f) during the methylation-demethylation experiment for sediment 1

Figure 9 presents the predictive uncertainty plots obtained by generating an ensemble of sorption and methylation model runs using the parameters sets from MCMC. Model reduction from kinetic to equilibrium for Hg reduction and from Monod for first-order kinetics for demethylation was found to be adequate as the model simulation results explain the experimental data well for both sorption and methylation experiments. The parameter estimates and thus predictions benefit from the joint fitting of sorption and methylation datasets and estimating all parameters simultaneously.

4.2.2. Sediment 2

Parameters for the fast-site sorption for Hg and MeHg considered by Schwartz et al. (2022) exhibited high ambiguity as they contain a null space with a distinctive ratio of forward and reverse rate constants. In the improved model, sorption of Hg and MeHg on Sediment 2 is modeled as two-site sorption, i.e. equilibrium and kinetic sorption. Equilibrium sorption constants for Hg and MeHg are represented by $K_{1-2}[-]$ and $K_{7-8}[-]$, respectively. Similar to Sediment 1, Hg reduction in sediment 2 is modeled as an equilibrium process with the equilibrium constant as $K_{5-6}\,[-]$. Guo et al. (2019) showed that the uncertainty in the thermodynamic constants for equilibrium processes has an outsized impact on the output uncertainties, hence it is critical to obtain global uncertainty estimates for these constants. The joint distribution of estimated parameters in Figure 10 are well-constrained and unimodal. The summary statistics of estimated parameters are presented in Table 2. Predictive uncertainty plots in Figure 11 show good agreement between model simulations and experimental data for both sorption and methylation experiments.

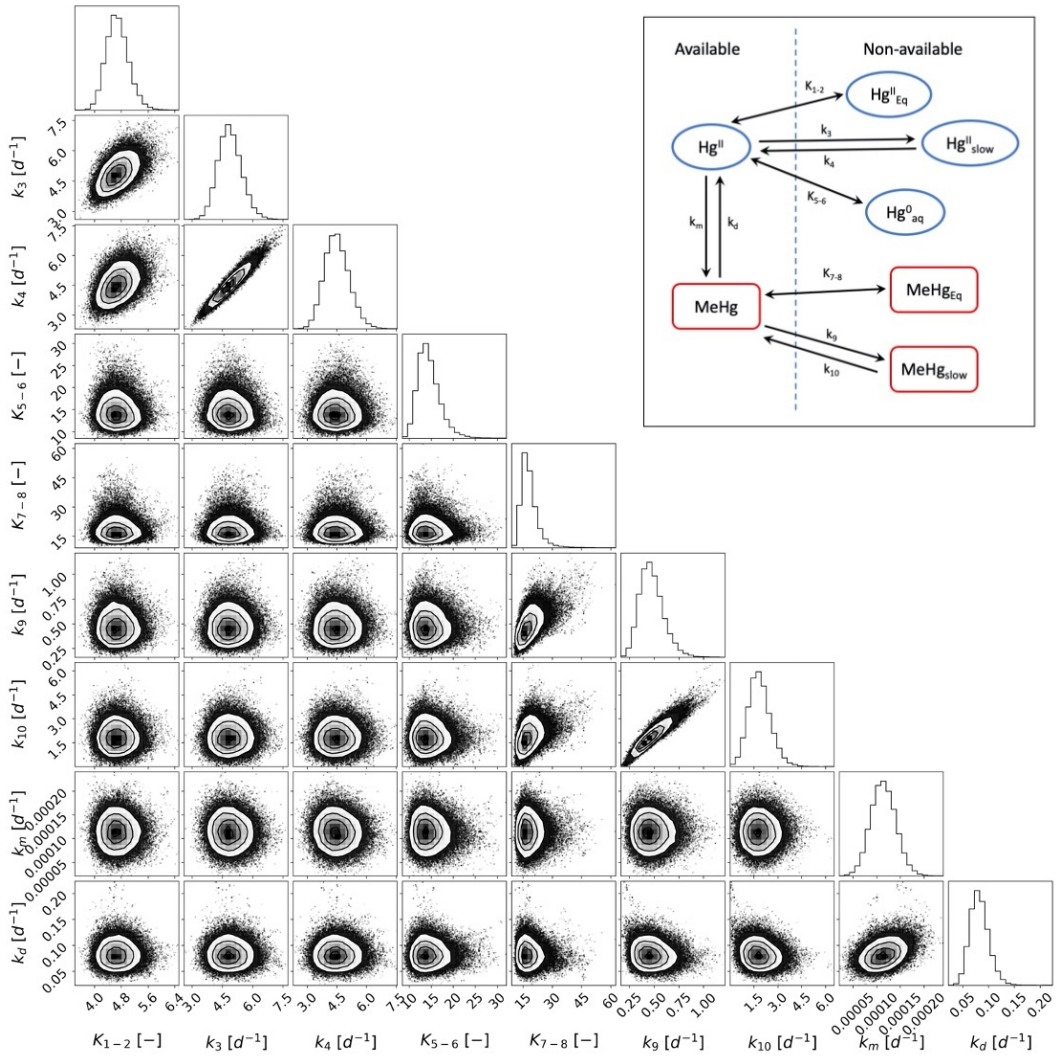

Figure 10: Model description (top right) and joint distributions of parameters obtained from MCMC for the improved model for sediment 2

Table 2: Summary statistics of parameters estimated from MCMC for the improved model for sediment 1

Parameter	5th	25th	Median	75th	95th
$K_{1-2}[-]$	4.18	4.46	4.67	4.90	5.27
$k_3[d^{-1}]$	3.98	4.48	4.85	5.25	5.89
$k_4[d^{-1}]$	3.55	4.08	4.48	4.91	5.59
$K_{5-6}[-]$	11.10	12.75	14.16	15.9	19.2
$K_{7-8}[-]$	13.19	15.38	17.41	20.07	26.15
$k_9[d^{-1}]$	3.03e-1	3.91e-1	4.64e-1	5.48e-1	6.95e-1
$k_{10}[d^{-1}]$	8.37e-1	1.39	1.81	2.28	3.09
$k_m[d^{-1}]$	7.23e-5	9.64e-5	11.38e-5	13.19e-5	15.85e-5
$k_d[d^{-1}]$	5.57e-2	7.01e-2	8.14e-2	9.38e-2	11.46e-2

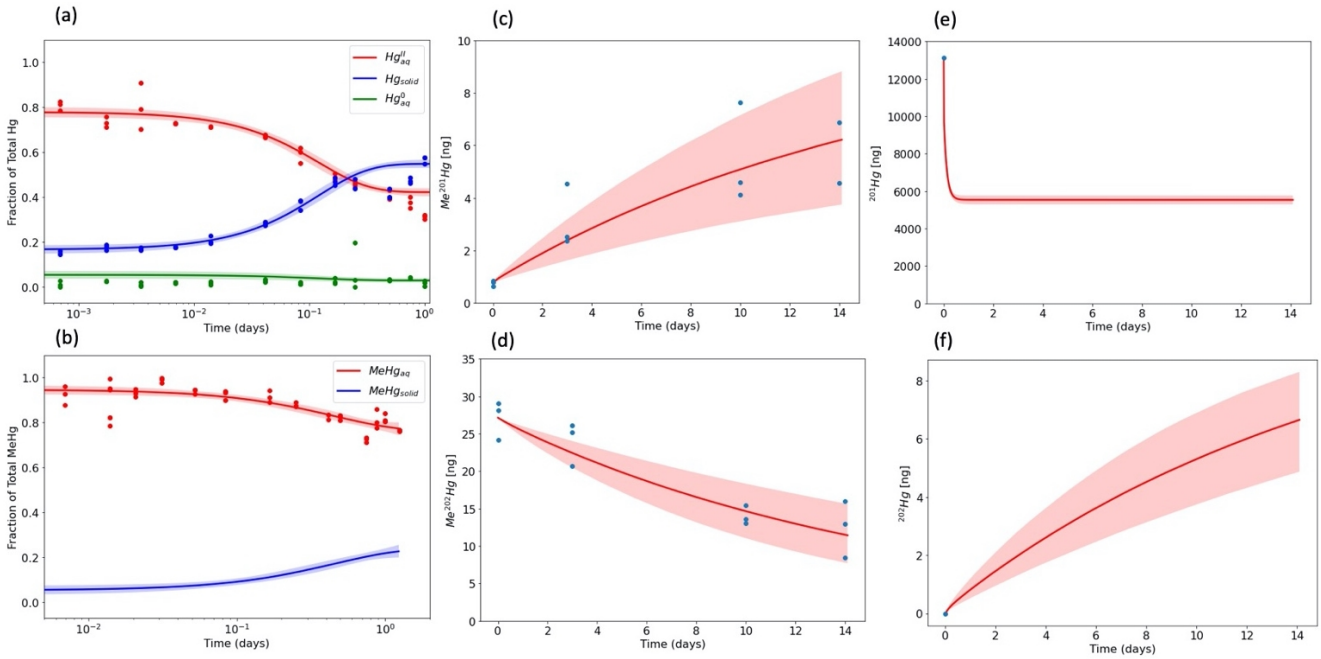

Figure 11: Median (solid line), band of 2.5th and 97.5th percentiles (shaded region) of predictions and experimental data (solid dots) for Hg sorption and reduction (gaseous phase is not shown) (a), MeHg sorption (b), and methylation-demethylation experiment (c - d), along with the predicted concentration history of total dissolved of ^{201}Hg (e) and ^{202}Hg (f) during the methylation-demethylation experiment for Sediment 2

5.3. Summary and Conclusions

In this paper, we proposed Bayesian joint fitting, a parameter-estimation workflow, for biogeochemical systems with two main advancements from traditional methods: 1) simultaneous fitting of datasets from multiple experiments characterizing competing subprocesses within the system, 2) mapping full joint distribution of parameters using MCMC. The efficacy of the proposed method was demonstrated with mercury methylation as a use case. The method was deployed to reinterpret recently published datasets (Schwartz et al., 2021b) characterizing mercury methylation on aquatic sediments under the Transient Availability Model (TAM) framework (Olsen et al., 2018; Schwartz et al., 2022). Rigorous estimation of parameter uncertainties and improvement in the TAM framework were achieved.

Simultaneous fitting of datasets from sorption and methylation experiments to estimate all TAM parameters together comprehensively captured interactions between sorption and methylation processes. This approach allowed the inclusion of the measurement uncertainties in the sorption experiments (for both Hg and MeHg) into methylation parameters in the TAM model framework. Another advantage of simultaneously fitting datasets is sorption parameters were informed by datasets from both sorption and methylation experiments.

Mapping full joint distributions of parameters using MCMC yielded global optimal parameters and robust uncertainty estimates. Additionally, it revealed deficiencies in the existing model

structure which eluded first-order error estimates. For example, the identification of null spaces in the original sorption model (Schwartz et al., 2022) in Sediment 2 and the Hg-reduction model for both sediments proved valuable in simplifying the model from kinetic to equilibrium, thus reducing the parameter uncertainty arising due to over-parameterization. Similarly, null space in parameters for Monod demethylation in Schwartz et al. (2022) model suggested replacing it with first-order kinetics. Note that lumping null space parameters into a single parameter is one of the many ways of model reduction. This inverse-modeling-based approach simplifies the model with null-space identification without compromising on the goodness of fit and prediction uncertainties. The different fast sorption dynamics of the finer-grained Sediment 1 and coarser-grained Sediment 2 is consistent with reduced access to sorption sites due to low diffusion coefficients in Sediment 2. Such insights can be helpful to guide future experiments for better resolving processes that exert control on Hg methylation-MeHg demethylation dynamics in environmental systems. For example, the MeHg concentrations measured in samples is the net result of the opposing processes of Hg methylation and MeHg demethylation. The simultaneous fitting approach discriminated among competing models describing these processes and identified parameters with greater relative uncertainty which, in turn, will inform future data gathering efforts to design experiments that will decrease uncertainty in those parameters. Other approaches include using theoretical measures like Akaike Information Criterion or Bayesian Information Criterion to trade-off the goodness of fit for the model simplicity.

Bayesian inference from experimental datasets (Schwartz et al., 2021b) revealed different methylation and sorption dynamics for Sediment 1 and Sediment 2. In Sediment 1, two-site kinetic sorption (fast and slow) explained the datasets well. In Sediment 2, data did not capture kinetic behavior for fast sorption making the associated kinetic parameters unidentifiable. The equilibrium sorption along with slow kinetic sorption resulted in a good fit between the model and data. For the methylation experiment in Sediment 1, Monod methylation and first-order demethylation gave a decent fit to the data with unique parameter estimates. The dataset was unable to uniquely identify Monod parameters for demethylation. In Sediment 2, first-order kinetics for both methylation and demethylation offered a good match with the data.

In summary, the proposed method of joint fitting of multiple-experiment datasets in the Bayesian framework and mapping full joint distributions using MCMC were shown to be effective in improving the parameterization of biogeochemical models, quantifying the uncertainties in parameters and outputs, and evaluating different model structures. This approach can be beneficial particularly in a system with multiple competing reactions taking place at different timescales. Insights into parameter space through joint probability distributions coupled with domain knowledge guides model improvements. Full quantification of uncertainties informs the design of future experiments targeted at constraining poorly constrained parameters, eliminating multimodality or dealing with parameter degeneracy. Improved model structures and robust uncertainty estimates offer better understanding of underlying mechanisms and reliable predictions of fate of metals and nutrients in the environment.

Parameter estimation using MCMC will not be suitable for models with high runtime as MCMC requires large number of model runs, raising the computational cost. However, typical reaction networks are ODEs and even a complex reaction network is relatively fast to solve. Additionally, with an increased access to computational resources, there is no reason why researcher should not opt for robust uncertainty estimates using MCMC which offers flexibility of analyzing multiple experiments together and also guide domain-knowledge-based model improvements in the process.

The workflow for this approach is coded in Python and scripts are provided in the mode-data archive at Rathore and Painter (2021). The modular nature of the workflow allows for inclusion of additional experimental data or a new reaction to the reaction network, conveniently.

Acknowledgments

This work was funded by the U.S. Department of Energy, Office of Science, Biological and Environmental Research, Subsurface Biogeochemical Research (SBR) Program, and is a product of the Critical Interfaces Science Focus Area (SFA) at ORNL and the IDEAS-Watersheds project. This research used resources of the Compute and Data Environment for Science (CADES) at the Oak Ridge National Laboratory, which is supported by the Office of Science of the U.S. Department of Energy under Contract No. DE-AC05-00OR22725. We thank the editor and anonymous reviewer for their constructive feedback on the paper.

References:

Arhonditsis, G.B., Papantou, D., Zhang, W., Perhar, G., Massos, E., Shi, M., 2008. Bayesian calibration of mechanistic aquatic biogeochemical models and benefits for environmental management. Journal of Marine Systems 73(1) 8-30. doi:https://doi.org/10.1016/j.jmarsys.2007.07.004

Avramescu, M.-L., Yumvihoze, E., Hintelmann, H., Ridal, J., Fortin, D., R.S. Lean, D., 2011. Biogeochemical factors influencing net mercury methylation in contaminated freshwater sediments from the St. Lawrence River in Cornwall, Ontario, Canada. Science of The Total Environment 409(5) 968-978. doi:https://doi.org/10.1016/j.scitotenv.2010.11.016

Beck, M.B., 1987. Water quality modeling: A review of the analysis of uncertainty. Water Resources Research 23(8) 1393-1442. doi:https://doi.org/10.1029/WR023i008p01393

Brooks, S.C., Southworth, G.R., 2011. History of mercury use and environmental contamination at the Oak Ridge Y-12 Plant. Environmental Pollution 159(1) 219-228. doi:https://doi.org/10.1016/j.envpol.2010.09.009

Chen, C.Y., Folt, C.L., 2000. Bioaccumulation and Diminution of Arsenic and Lead in a Freshwater Food Web. Environmental Science & Technology 34(18) 3878-3884. doi:10.1021/es991070c

Clarkson, T.W., Magos, L., Myers, G.J., 2003. The Toxicology of Mercury — Current Exposures and Clinical Manifestations. New England Journal of Medicine 349(18) 1731-1737. doi:10.1056/NEJMra022471

Davoudabadi, M.J., Pagendam, D., Drovandi, C., Baldock, J., White, G., 2021. Advanced Bayesian approaches for state-space models with a case study on soil carbon sequestration. Environmental Modelling & Software 136 104919. doi:https://doi.org/10.1016/j.envsoft.2020.104919

Eckley, C.S., Gilmour, C.C., Janssen, S., Luxton, T.P., Randall, P.M., Whalin, L., Austin, C., 2020. The assessment and remediation of mercury contaminated sites: A review of current approaches. Science of The Total Environment 707 136031. doi:https://doi.org/10.1016/j.scitotenv.2019.136031

Evers, D.C., Han, Y.-J., Driscoll, C.T., Kamman, N.C., Goodale, M.W., Lambert, K.F., Holsen, T.M., Chen, C.Y., Clair, T.A., Butler, T., 2007. Biological Mercury Hotspots in the Northeastern United States and Southeastern Canada. BioScience 57(1) 29-43. doi:10.1641/B570107

Gelman, A., Rubin, D.B.J.S.s., 1992. Inference from iterative simulation using multiple sequences. Statistical Science 7(4) 457-472.

646 Goodyear, K.L., McNeill, S., 1999. Bioaccumulation of heavy metals by aquatic macro-
647 invertebrates of different feeding guilds: a review. Science of The Total Environment 229(1) 1-
648 19. doi:10.1016/S0048-9697(99)00051-0

649 Guo, L., Painter, S.L., Brooks, S.C., Parks, J.M., Smith, J.C., 2019. A probabilistic perspective on
650 thermodynamic parameter uncertainties: Understanding aqueous speciation of mercury.
651 Geochimica et Cosmochimica Acta 263 108-121.

652 Haggerty, R., Argerich, A., Martí, E., 2008. Development of a "smart" tracer for the assessment
653 of microbiological activity and sediment-water interaction in natural waters: The resazurin-
654 resorufin system. Water Resources Research 44(4). doi:10.1029/2007wr006670

655 Hintelmann, H., Keppel-Jones, K., Evans, R.D., 2000. Constants of mercury methylation and
656 demethylation rates in sediments and comparison of tracer and ambient mercury availability.
657 Environmental Toxicology and Chemistry 19(9) 2204-2211. doi:10.1002/etc.5620190909

658 Horowitz, A.J., 1991. A primer on sediment-trace element chemistry, Open-File Report, 2nd.
659 ed., rev. ed.

660 Jonsson, S., Skyllberg, U., Nilsson, M.B., Westlund, P.-O., Shchukarev, A., Lundberg, E., Björn, E.,
661 2012. Mercury Methylation Rates for Geochemically Relevant HgII Species in Sediments.
662 Environmental Science & Technology 46(21) 11653-11659. doi:10.1021/es3015327

663 Kelleher, C., Ward, A., Knapp, J.L.A., Blaen, P.J., Kurz, M.J., Drummond, J.D., Zarnetske, J.P.,
664 Hannah, D.M., Mendoza-Lera, C., Schmadel, N.M., Datry, T., Lewandowski, J., Milner, A.M.,
665 Krause, S., 2019. Exploring Tracer Information and Model Framework Trade-Offs to Improve
666 Estimation of Stream Transient Storage Processes. Water Resources Research 55(4) 3481-3501.
667 doi:10.1029/2018wr023585

668 Knapp, J.L.A., Cirpka, O.A., 2017. Determination of hyporheic travel time distributions and other
669 parameters from concurrent conservative and reactive tracer tests by local-in-global
670 optimization. Water Resources Research 53(6) 4984-5001. doi:10.1002/2017wr020734

671 Laloy, E., Vrugt, J.A., 2012. High-dimensional posterior exploration of hydrologic models using
672 multiple-try DREAM(ZS) and high-performance computing. Water Resources Research 48(1).
673 doi:10.1029/2011wr010608

674 Lemke, D., González-Pinzón, R., Liao, Z., Wöhling, T., Osenbrück, K., Haggerty, R., Cirpka, O.J.H.,
675 Sciences, E.S., 2014. Sorption and transformation of the reactive tracers resazurin and resorufin
676 in natural river sediments. 18(8).

677 Lemke, D., Liao, Z., Wöhling, T., Osenbrück, K., Cirpka, O., 2013. Concurrent conservative and
678 reactive tracer tests in a stream undergoing hyporheic exchange. Water Resources Research
679 49(5) 3024-3037. doi:10.1002/wrcr.20277

Liao, Z., Lemke, D., Osenbrück, K., Cirpka, O.A., 2013. Modeling and inverting reactive stream tracers undergoing two-site sorption and decay in the hyporheic zone. 49(6) 3406-3422. doi:10.1002/wrcr.20276

Liem-Nguyen, V., Jonsson, S., Skyllberg, U., Nilsson, M.B., Andersson, A., Lundberg, E., Björn, E., 2016. Effects of Nutrient Loading and Mercury Chemical Speciation on the Formation and Degradation of Methylmercury in Estuarine Sediment. Environmental Science & Technology 50(13) 6983-6990. doi:10.1021/acs.est.6b01567

Luo, J., Cirpka, O.A., Fienen, M.N., Wu, W.-m., Mehlhorn, T.L., Carley, J., Jardine, P.M., Criddle, C.S., Kitanidis, P.K., 2006. A parametric transfer function methodology for analyzing reactive transport in nonuniform flow. Journal of Contaminant Hydrology 83(1) 27-41. doi:https://doi.org/10.1016/j.jconhyd.2005.11.001

Marschmann, G.L., Pagel, H., Kügler, P., Streck, T., 2019. Equifinality, sloppiness, and emergent structures of mechanistic soil biogeochemical models. Environmental Modelling & Software 122 104518.

Mason, R.P., Laporte, J.M., Andres, S., 2000. Factors Controlling the Bioaccumulation of Mercury, Methylmercury, Arsenic, Selenium, and Cadmium by Freshwater Invertebrates and Fish. Archives of Environmental Contamination and Toxicology 38(3) 283-297. doi:10.1007/s002449910038

Mergler, D., Anderson, H.A., Chan, L.H.M., Mahaffey, K.R., Murray, M., Sakamoto, M., Stern, A.H., 2007. Methylmercury Exposure and Health Effects in Humans: A Worldwide Concern. AMBIO: A Journal of the Human Environment 36(1) 3-11, 19.

Mitchell, C.P.J., Gilmour, C.C., 2008. Methylmercury production in a Chesapeake Bay salt marsh. Journal of Geophysical Research: Biogeosciences 113(G2). doi:10.1029/2008JG000765

Neumann, M.B., Gujer, W., 2008. Underestimation of Uncertainty in Statistical Regression of Environmental Models: Influence of Model Structure Uncertainty. Environmental Science & Technology 42(11) 4037-4043. doi:10.1021/es702397q

Olsen, T.A., Muller, K.A., Painter, S.L., Brooks, S.C., 2018. Kinetics of Methylmercury Production Revisited. Environmental Science & Technology 52(4) 2063-2070. doi:10.1021/acs.est.7b05152

Rathore, S.S., Painter, S.L., 2021. Model-Data for Joint Estimation of Biogeochemical Model Parameters from Multiple Experiments: A Bayesian Approach Applied to Mercury Methylation. ORNL Mercury Science Focus Area (SFA) Data Collection. doi:10.12769/1805731

Riscassi, A., Miller, C., Brooks, S., 2016. Seasonal and flow-driven dynamics of particulate and dissolved mercury and methylmercury in a stream impacted by an industrial mercury source. Environmental Toxicology and Chemistry 35(6) 1386-1400. doi:10.1002/etc.3310

Rodŕiguez Martín-Doimeadios, R.C., Tessier, E., Amouroux, D., Guyoneaud, R., Duran, R., Caumette, P., Donard, O.F.X., 2004. Mercury methylation/demethylation and volatilization pathways in estuarine sediment slurries using species-specific enriched stable isotopes. Marine Chemistry 90(1) 107-123. doi:https://doi.org/10.1016/j.marchem.2004.02.022

Schwartz, G.E., Muller, K.A., Rathore, S.S., Wilpiszeski, R.L., Carrell, A.A., Cregger, M.A., Elias, D.A., Podar, M., Painter, S.L., Brooks, S.C., 2021a. Incorporating Variable Sediment Microbial Activity into Methylmercury Production Kinetics Modeling.

Schwartz, G.E., Muller, K.A., Rathore, S.S., Wilpiszeski, R.L., Carrell, A.A., Cregger, M.A., Elias, D.A., Podar, M., Painter, S.L., Brooks, S.C., 2022. Incorporating concentration-dependent sediment microbial activity into methylmercury production kinetics modeling. Environmental Science: Processes & Impacts.

Schwartz, G.E., Muller, K.A., Wilpiszeski, R.L., Carrell, A.A., Cregger, M.A., Elias, D.A., Podar, M., Brooks, S.C., 2021b. [Dataset] Incorporating Variable Sediment Microbial Activity into Methylmercury Production Kinetics Modeling doi:10.12769/1797572

Schwartz, G.E., Olsen, T.A., Muller, K.A., Brooks, S.C., 2019. Ecosystem Controls on Methylmercury Production by Periphyton Biofilms in a Contaminated Stream: Implications for Predictive Modeling. Environmental Toxicology and Chemistry 38(11) 2426-2435. doi:https://doi.org/10.1002/etc.4551

Shockley, E.M., Vrugt, J.A., Lopez, C.F., 2018. PyDREAM: high-dimensional parameter inference for biological models in python. Bioinformatics (Oxford, England) 34(4) 695-697. doi:10.1093/bioinformatics/btx626

van Oijen, M., Cameron, D.R., Butterbach-Bahl, K., Farahbakhshazad, N., Jansson, P.E., Kiese, R., Rahn, K.H., Werner, C., Yeluripati, J.B., 2011. A Bayesian framework for model calibration, comparison and analysis: Application to four models for the biogeochemistry of a Norway spruce forest. Agricultural and Forest Meteorology 151(12) 1609-1621. doi:https://doi.org/10.1016/j.agrformet.2011.06.017

van Turnhout, A.G., Kleerebezem, R., Heimovaara, T.J., 2016. A toolbox to find the best mechanistic model to predict the behavior of environmental systems. Environmental Modelling & Software 83 344-355. doi:https://doi.org/10.1016/j.envsoft.2016.05.002

Vrugt, J.A., Hyman, J.M., Robinson, B.A., Higdon, D., Ter Braak, C.J., Diks, C.G., 2008. Accelerating Markov chain Monte Carlo simulation by differential evolution with self-adaptive randomized subspace sampling. Los Alamos National Lab.(LANL), Los Alamos, NM (United States).

Ward, D.M., Nislow, K.H., Folt, C.L., 2010. Bioaccumulation syndrome: identifying factors that make some stream food webs prone to elevated mercury bioaccumulation. Annals of the New York Academy of Sciences 1195 62-83. doi:10.1111/j.1749-6632.2010.05456.x

Zhang, W., Arhonditsis, G.B., 2009. A Bayesian hierarchical framework for calibrating aquatic biogeochemical models. Ecological Modelling 220(18) 2142-2161. doi:https://doi.org/10.1016/j.ecolmodel.2009.05.023

Zhao, Y., Rathore, S.S., Liu, M., Luo, J., 2018. Joint Bayesian inversion for analyzing conservative and reactive breakthrough curves. Journal of Hydrology 567 446-456. doi:https://doi.org/10.1016/j.jhydrol.2018.10.029

Appendix-A

Here we present mathematical equations for improved models for mercury methylation on aquatic sediments presented in this manuscript. For variables are described in the main text of the manuscript.

Sediment 1:

(1) $\frac{d[Hg]}{dt} = \frac{-k_{mmax}}{K_{mhs} + [Hg]}[Hg] + k_d\,[MeHg] - k_1[Hg] + k_2[Hg_f] - k_3[Hg] + k_4\,[Hg_s]$

(2) $\frac{d[MeHg]}{dt} = \frac{k_{mmax}}{K_{mhs} + [Hg]}[Hg] - k_d\,[MeHg] - k_7[MeHg] + k_8[MeHg_f] - k_9[MeHg] + k_{10}[MeHg_s]$

(3) $\frac{d[Hg_f]}{dt} = k_1[Hg] - k_2[Hg_f]$

(4) $\frac{d[Hg_s]}{dt} = k_3[Hg] - k_4\,[Hg_s]$

(5) $\frac{d[MeHg_f]}{dt} = k_7[MeHg] - k_8[MeHg_f]$

(6) $\frac{d[MeHg_s]}{dt} = k_9[MeHg] - k_{10}[MeHg_s]$

(7) $[Hg] = K_{5-6}[Hg^0]$

Sediment 2:

(1) $\frac{d[Hg]}{dt} = -k_m[Hg] + k_d\,[MeHg] - k_3[Hg] + k_4\,[Hg_s]$

(2) $\frac{d[MeHg]}{dt} = k_m[Hg] - k_d[MeHg] - k_9[MeHg] + k_{10}[MeHg_s]$

(3) $\frac{d[Hg_s]}{dt} = k_3[Hg] - k_4\,[Hg_s]$

(4) $\frac{d[MeHg_s]}{dt} = k_9[MeHg] - k_{10}[MeHg_s]$

(5) $[Hg] = K_{1-2}[Hg_f]$

(6) $[Hg] = K_{5-6}[Hg^0]$

(7) $[MeHg] = K_{7-8}[MeHg_f]$

Appendix-B

Example plots of residual distribution for the time series of $Me^{201}Hg$ and $Me^{202}Hg$ in methylation and demethylation experiments for both Sediment 1 and Sediment 2 are shown below.

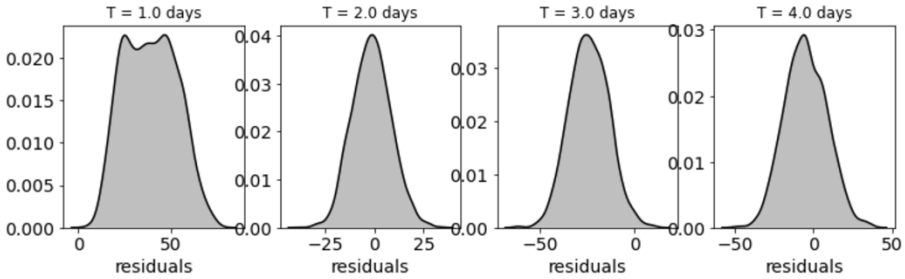

Figure B.1: Distribution of residuals for $Me^{201}Hg$ predictions are different timepoints for methylation experiment in Sediment 1

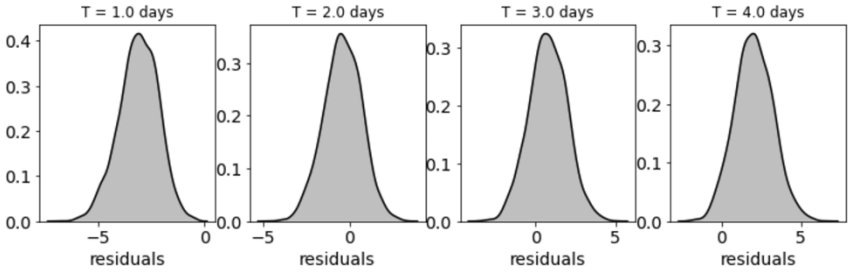

Figure B.2: Distribution of residuals for $Me^{202}Hg$ predictions are different timepoints for demethylation experiment in Sediment 1

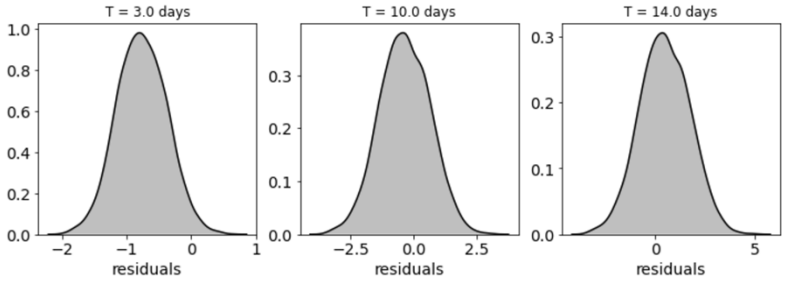

Figure B.3: Distribution of residuals for $Me^{201}Hg$ predictions are different timepoints for methylation experiment in Sediment 2

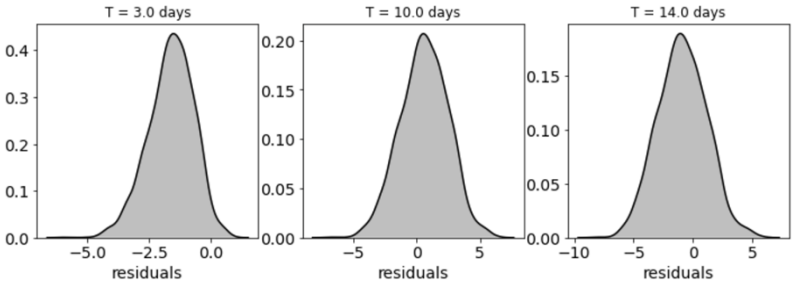

Figure B.4: Distribution of residuals for $Me^{202}Hg$ predictions are different timepoints for demethylation experiment in Sediment 2

803